# CONCERNS ABOUT A VARIANCE APPROACH TO X-RAY DIFFRACTOMETRIC ESTIMATION OF MICROFIBRIL ANGLE IN WOOD[1]

## Steve P. Verrill*†

Mathematical Statistician

## David E. Kretschmann†

Research General Engineer

## Victoria L. Herian†

Statistician

## Michael C. Wiemann†

Wood Anatomist
USDA Forest Products Laboratory
Madison, WI 53726

## Harry A. Alden

Wood Anatomist
College of Southern Maryland
Prince Frederick, MD 20678

**Abstract.** In this article, we raise three technical concerns about Evans' 1999 *Appita Journal* "variance approach" to estimating microfibril angle (MFA). The first concern is associated with the approximation of the variance of an X-ray intensity half-profile by a function of the MFA and the natural variability of the MFA. The second concern is associated with the approximation of the natural variability of the MFA by a function of the MFA. The third concern is associated with the fact that the variance approach was not designed to handle tilt in the fiber orientation. All three concerns are associated with potential biases in MFA estimates. We raise these three concerns so that other researchers interested in understanding, implementing, or extending the variance approach or in comparing the approach to other methods of estimating MFA will be aware of them.

*Keywords:* Microfibril angle estimation, bias, variance approach, cell rotation, cell tilt, cell cross-section, X-ray diffraction.

## INTRODUCTION

Microfibril angle (MFA) is the angle between the direction of crystalline cellulose fibrils in the cell wall and the longitudinal direction of the cell. There is strong belief that the MFA of the woody cell wall S2 layer is a critical factor in the mechanical behavior of wood (Megraw 1986). S2 MFA appears to have a significant influence on wood tensile strength, stiffness, and shrinkage (Harris and Meylan 1965; Cave and Walker 1994; Evans and Illic 2001). Thus, rapid estimation of MFA from the scanning of cores has been developed as a method for comparing and improving silvicultural practices and as a technique for identifying superior trees.

Evans (1999) provides theoretical justification for a variance approach to estimating MFA from X-ray diffraction patterns. In this article, we raise concerns about three aspects of that approach:

---

1. We believe that the justification for the base approximation

$$S^2 \approx \frac{\mu^2}{2} + \sigma^2$$

is not strong. (Here, $\mu$ denotes MFA, $\sigma$ denotes the natural variability of the MFA, and $S^2$ is defined in Section 2.)

2. An implementor of the approach must choose a function of $\mu$ with which to model $\sigma^2$. Evans (1999) proposed the general model

$$\sigma^2 = (k \times \mu)^2 + \sigma_{add}^2$$

and suggested that 1/3 and 6 might be reasonable choices for $k$ and $\sigma_{add}$. We demonstrate that biases in the MFA estimate can be sensitive to the choice of model for $\sigma^2$.

3. The 1999 variance approach was not designed to handle fiber tilt. We show that the method can perform poorly in the presence of tilt. (Some implementors of the variance approach have apparently developed extensions to the method that are intended to handle tilt. However, these methods have not yet been detailed in the open literature.)

We raise these three concerns so that other researchers interested in understanding, implementing, or extending the variance approach, or in comparing the approach to other methods of estimating MFA will be aware of them.

### VARIANCE APPROACH

Evans (1999) proposed the variance approach to estimating MFA and gave a detailed description of the method. Here we give a quick synopsis.

The procedure is based on X-ray diffraction techniques. The radial wall of a machined core is irradiated by a 0.2-mm-diameter X-ray beam, which produces a diffraction pattern on a back plane. In general, because of reflections from the 002 crystallographic planes in the cellulose microfibrils, two back plane bright spots are produced per wood cell face. Thus, cells with rectangular cross-sections yield eight back plane

bright spots, while those with hexagonal cross-sections produce 12 bright spots. These bright spot patterns are broadened by (among other factors) MFA variability and variabilities in cell rotation and tilt. These broadened intensity patterns can be evaluated along the $2\theta$ circle on the back plane (where $\theta$ is the Bragg angle). In Fig 1, we provide an example of this intensity profile. These profiles contain left and right halves that are more or less symmetric depending on wood cell rotation and tilt.

Evans (1999) argued that

$$S^2 \approx \frac{\mu^2}{2} + \sigma^2 \qquad (1)$$

where $S^2$ is the variability of either profile half, $\mu$ is the mean MFA, and $\sigma^2$ is the variability of MFA in the path of the beam. Evans proposed the additional approximation

$$\sigma^2 \approx f(\mu) \qquad (2)$$

for some function $f$. Taken together, Eqs 1 and 2 yield

$$S^2 \approx \frac{\mu^2}{2} + f(\mu) \qquad (3)$$

which, in principle, can be solved for $\mu$. To implement this procedure in practice requires a detailed assumption about $f(\mu)$.

Evans (1999) suggested that $\sigma^2$ could be replaced by

$$f(\mu) = \sigma_{mult}^2 + \sigma_{add}^2 = (k \times \mu)^2 + \sigma_{add}^2$$

Evans went on to suggest that reasonable values for $k$ might be 1/4 or 1/5 or Cave's 1/3 and a reasonable value for $\sigma_{add}$ might "lie in the range 6-10" degrees. He further stated that (as of 1999) he used $k = 1/3$ and $\sigma_{add} = 6$. In a personal communication (Evans 2008), he stated that he continued to use

$$\sigma^2 \approx f(\mu) = \left(\frac{\mu}{3}\right)^2 + 6^2 \qquad (4)$$

Combining Eqs 1 and 4, we obtain Evans' (1999) Eq 34:

MFAactive1

| 1 | 3.16e+001 | 2 | 3.16e+001 | 3 | 3.26e+001 | 4 | 3.38e+001 | 5 | | ID_min: | 1 | mss_min: | 9.44e+001 |
| mss1: | 9.44e+001 | mss2: | 1.21e+002 | mss3: | 1.21e+002 | mss4: | 1.13e+002 | mss5: | | mss_cut: | 9.49e+001 | | |

03ar1erX

| a: | 2.8433e+002 |
| b1: | 1.4417e+002 |
| b2: | 1.6389e+002 |
| mu1: | -3.8888e+001 |
| sigma1: | 4.3758e+001 |
| Initial 6 | Fit 6 |
| c,nc (-22.5) | c,c (0) |
| nc,c (22.5) | nc,nc (45) |
| MFA: | 3.1595e+001 |
| rot: | -6.3174e+001 |
| tilt: | -5.5727e+000 |
| sdFB_lp: | 2.4999e+001 |
| sdFB_rp: | 1.1365e+001 |
| sdRL_lp: | 1.0157e+001 |
| sdRL_rp: | 1.0005e+001 |
| a: | 3.0930e+002 |
| bFB: | 1.2423e+003 |
| bRL: | 8.5925e+002 |
| bRdL: | 8.9586e-001 |
| Initial 11 | Fit 11 |
| | Fit 11,4 |

intensity: 500.0, 450.0, 400.0, 350.0, 300.0

angle: -100.0, 0.0, 100.0, 200.0, 300.0

Load | 03ar1erX | Reset | Clear All | Clear | Zoom | Back | Next | Stop
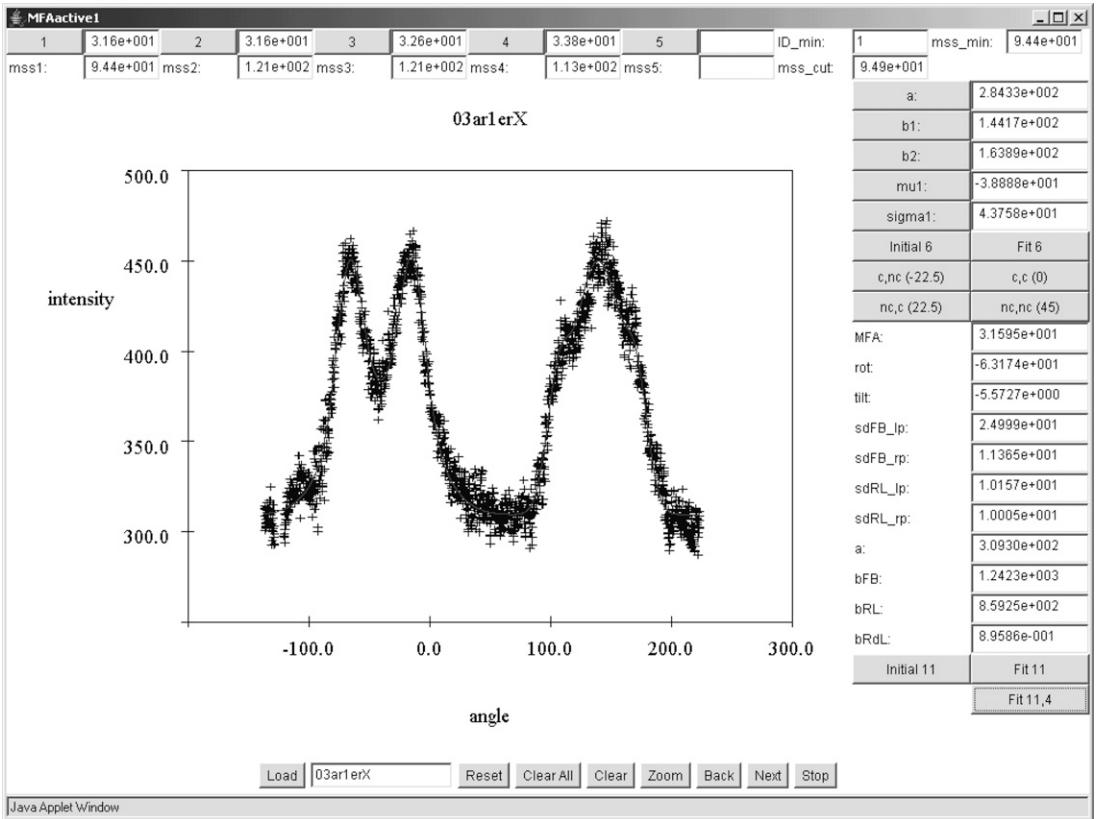
Java Applet Window

Figure 1.   The double-peaked half of the intensity profile corresponds (roughly) to the right half of the back plane. The single-peaked half of the profile corresponds (roughly) to the left half of the back plane. In this case, the X-ray apparatus was set up so that the minimum between the two halves of the profile would occur at 54.7° rather than 90°. For further explanation of this figure, see Fig 38 and the associated discussion in Verrill et al (2006).

$$\sqrt{\frac{18}{11}}\sqrt{S^2 - 6^2} \approx \mu \qquad (5)$$

This is the MFA estimate we evaluated in our simulations. Other variance approach estimates would be obtained if other values for $f(\mu)$ were used.

We have developed analytical and simulation tools that permit us to evaluate the quality of variance approach estimates. In the next section, we describe our simulation tools and report results of simulation experiments that were performed with these tools. These experiments helped us identify conditions under which the 1999 algorithm does not perform well.

Following that, we look at the theoretical basis for Eq 1 and identify two weaknesses in its derivation. Then, we evaluate biases that can occur when wood cells are tilted. Next, we identify good experimental practices that new implementors of the approach can use to guard against poor performance. We also identify naturally occurring sources of variability that can cause problems for the unmodified 1999 algorithm, and that cannot be easily circumvented. Finally, we consider Eq 2 and biases that can occur when the approximation is not correct.

SIMULATION TOOLS AND RESULTS

In the course of developing MFA X-ray diffraction techniques (Verrill et al 2001, 2006, 2011), we developed computational tools that permit us to calculate the back plane locations of the

unbroadened bright spots for rectangular and hexagonal wood cell cross-sections and many MFA/rotation/tilt combinations. Our methods are based on extensions of an equation first derived by Cave (1966). For rectangular cross-sections, the techniques are described in Appendix A of Verrill et al (2006). For hexagonal cross-sections, the techniques are described in Appendix A of Verrill et al (2010a). We used these methods to evaluate the performance of the variance approach to estimating MFA. Under the assumption of Gaussian MFA variability and given the standard deviation of the Gaussian distribution (we used Eq 4 as the value for MFA variance), we performed Monte Carlo draws from the MFA distribution and then calculated the corresponding azimuthal coordinates of the bright spots on the back plane.

Given 10,000 Monte Carlo draws, we obtained back plane X-ray intensity profiles. In the rectangular case, for example, each draw of MFA yielded the angular locations of eight bright spots on the back plane of the X-ray apparatus (Verrill et al 2006). These angles were accumulated in a frequency diagram (histogram) across 10,000 draws, and this diagram constituted the simulated X-ray intensity profile. We used these profiles to calculate variance approach estimates of MFAs and then compared these to the true generating MFAs. This permitted us to estimate biases associated with the variance approach. In addition, we broke the variability of the profiles into between-peak (in the rectangular case, eight intensity peaks are associated with the mean locations of the eight bright spots) and within-peak portions and thus analyzed the quality of approximations that led to Evans' (1999) Eq 29.

We also calculated the standard deviations associated with the peaks and compared these with values obtained from Evans' Eq 14. The FORTRAN code that formed the basis for these simulations is reported by Verrill et al (2010a). Results from these simulations are reported in Tables 1-50 of Verrill et al (2010b). PDFs of the article and tables are reported by Verrill et al (2010b). Biases in the variance approach estimates are reported in Tables 21-25 (rectangular cross-sections) and 46-50 (hexagonal cross-

sections) of Verrill et al (2010b). Biases are plotted in Figs 2-29 of Verrill et al (2010a). Figure 2 shows an example of these plots.

For larger cell tilts and larger MFAs, biases are significant. For example, for a rectangular cross-section, 15° rotation, 20° tilt, and 40° MFA, the full-profile bias (using both sets of peaks) is 5.9°, a 15% upward bias. The left half-profile (LHP) bias (using only the left set of peaks) is 10.1°, a 25% bias. For a hexagonal cross-section, 0° rotation, 20° tilt, and 40° MFA, the bias (both full-profile and half-profile) is 7.1°, an 18% bias. In general, biases increase as tilt and MFA increase.

As part of a more general simulation study, Sarén and Serimaa (2006) approximated the bias in the variance approach estimate of MFA for $\mu = 10$ and tilt = 2, 5, 10, 20, and 45°. Their estimated bias values are larger than ours.

We note that our simulations are not complete. Our methods permit tilt of the original $z$ axis of a cell toward the $x$ axis followed by rotation around the original $z$ axis (Fig 3). This permits the longitudinal axis of the cell to point in any direction, but it does not permit free rotation of the cell around that axis. We were led to this model by physical considerations associated with our X-ray apparatus (Verrill et al 2006). However, our model does not cover all possible
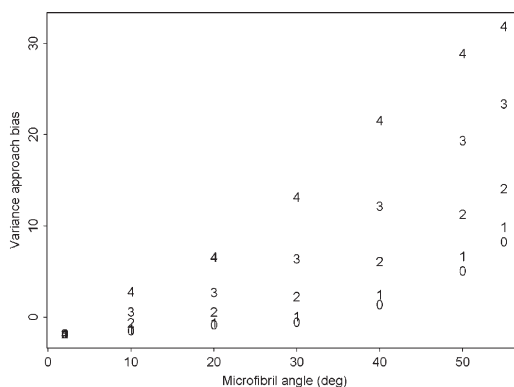


Figure 2. Full-profile variance approach biases vs true microfibril angle. Biases and microfibril angles are reported in degrees. 15° wood cell rotation. 0 = 0° tilt; 1 = 10° tilt; 2 = 20° tilt; 3 = 30° tilt; 4 = 40° tilt.
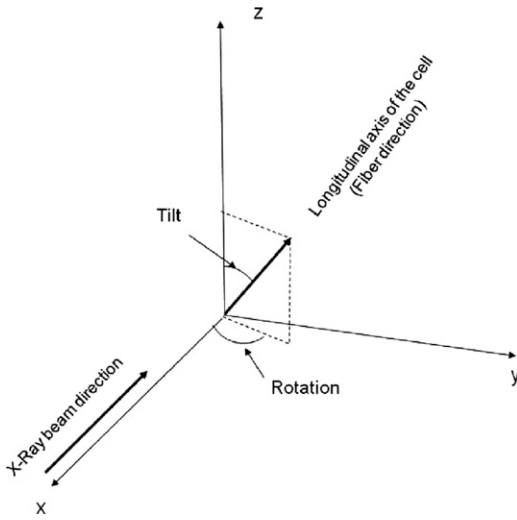
Figure 3.    Tilt and rotation of wood cell.

configurations. Furthermore, in reality, cell cross-sections can be quadrilateral, pentagonal, hexagonal, elliptical, or other forms and we have only modeled regular hexagons. In addition, in some circumstances, tangential and radial cell walls can differ significantly in thickness. In such circumstances, bright spots associated with thicker walls should be accentuated. In the current simulation, we assumed that cell walls are equal in thickness. Still, for the purposes of this article, our simulations are sufficient to highlight possible problems with the 1999 algorithm.

### PROBLEMS WITH SEVERAL VARIANCE APPROACH APPROXIMATIONS

Biases in the variance approach estimates result from approximations made in the course of the method's development and from the fact that the variance approach was not designed to handle tilt. In this section, we focus on Eq 1. In the next two sections, we focus on tilt. In the following section, we focus on Eq 2.

In this section, we revisit a portion of the theoretical development in Evans (1999). We focus on Eq 14-29 of that article.

Evans assumes that a wood cell has $J$ faces at angles $90 + \alpha_0 + 2\pi j / J, j = 0, \ldots, J - 1$ to

the incoming X-ray beam ($\alpha_0$ is the rotation of the front face away from perpendicular to the incoming beam). He further assumes (his Eq 12) that the contribution of the $j$th face to the (left or right half of the) back plane intensity profile is

$$I_j = \frac{1}{\sqrt{2\pi}} \frac{1}{\delta_j} \exp\left( \frac{(\phi - \phi_j)^2}{2\delta_j^2} \right) \qquad (6)$$

where $\phi$ denotes azimuthal angle, $\phi_j$ is the bright spot associated with the $j$th face for the half-profile (left or right) under consideration, and $\delta_j$ is the standard deviation of the broadened peak associated with the $j$th bright spot.

This normality assumption is presumably only approximately appropriate. Peura et al (2005, 2008a, 2008b) and Sarén et al (2001) found that MFA distributions both within single cells and across cells in a growth ring are right-skewed. (They restricted their attention to earlywood.) We found (Fig 4) that even if the generating MFA distribution for a face is normal, in general, the resulting back plane intensity distribution associated with that face is not. However, as we will see, the normality assumption is not needed for development of a variance approach to MFA estimation.

Given Eq 6, Evans notes that the mean bright spot location associated with the left or right back plane half-profile under consideration is (his Eq 17)

$$\bar{\phi} \equiv \sum_{J=0}^{J-1} \int_{-\infty}^{\infty} \frac{\phi I_j}{J} d\phi \qquad (7)$$

The variance of the half-profile is (his Eq 16)

$$S^2 \equiv \frac{\sum_{J=0}^{J-1} \int_{-\infty}^{\infty} (\phi - \bar{\phi})^2 I_j d\phi}{J} \qquad (8)$$

Evans makes an argument in his Eqs 18-25 that yields

$$S^2 = \sum_{j=0}^{J-1} \frac{\left(\phi_j - \frac{\pi}{2}\right)^2}{J} + \sum_{j=0}^{J-1} \frac{\delta_j^2}{J} \qquad (9)$$

Here we present a standard statistical argument that yields a similar conclusion.
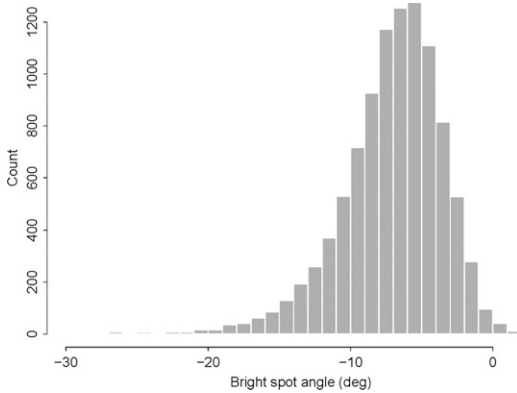
Figure 4. Histogram of the broadened left half-profile bright spot associated with the left face of a rectangular wood cell when cell rotation = 0°, cell tilt = 0°, and microfibril angle = 30°. The skewness of this distribution was −1.28. This figure was generated by calculating left half-profile, left face bright spot locations associated with 10,000 microfibril angle draws from a Gaussian distribution centered at 30° with variance $(30/3)^2 + 6$.

Suppose that, for a given half-profile (left or right), $y_{k1}, \ldots, y_{kJ}$ are the bright spot locations associated with the $k$ th draw of an MFA from the assumed MFA distribution (Evans assumed a distribution with mean $\mu$ and variance $\sigma^2$).

In cases of large MFA/tilt, a $y_{kj}$ might be missing. That is, there might be no reflections from a face.

Assume there are $n$ draws from the MFA distribution and that there are $n_j$ $y_{ij}$'s for $j = 1, \ldots, J$. For many tilt, rotation, MFA combinations, we will have $n_1 = \cdots = n_J = n$. However in some cases, because of lack of reflections from a face in some draws, we will have $n_j < n$ for some $j$.

**Define**

$$\bar{y}_{\cdot j} \equiv \sum_{i=1}^{n_j} \frac{y_{ij}}{n_j}$$

This is the mean bright spot location for the $j$ th peak in the half-profile.

The mean bright spot location for the half-profile will be

$$\bar{y}_{\cdot\cdot} \equiv \sum_{j=1}^{J} \frac{n_j \bar{y}_{\cdot j}}{n_{tot}}$$

where $n_{tot} = n_1 + \cdots + n_J$.

The variance of bright spot locations around this mean will be

$$
\begin{aligned}
S^2 &\equiv \sum_{j=1}^{J} \sum_{i=1}^{n_j} \frac{\left(y_{ij} - \bar{y}_{\cdot\cdot}\right)^2}{n_{tot}} \\
&= \sum_{j=1}^{J} \sum_{i=1}^{n_j} \frac{\left(y_{ij} - \bar{y}_{\cdot j} + \bar{y}_{\cdot j} - \bar{y}_{\cdot\cdot}\right)^2}{n_{tot}} \\
&= \sum_{j=1}^{J} \sum_{i=1}^{n_j} \frac{\left(\left(y_{ij} - \bar{y}_{\cdot j}\right)^2 + 2 \times \left(y_{ij} - \bar{y}_{\cdot j}\right)\left(\bar{y}_{\cdot j} - \bar{y}_{\cdot\cdot}\right) + \left(\bar{y}_{\cdot j} - \bar{y}_{\cdot\cdot}\right)^2\right)}{n_{tot}} \\
&= \sum_{j=1}^{J} \frac{\left(\sum_{i=1}^{n_j}\left(y_{ij} - \bar{y}_{\cdot j}\right)^2 + 2 \times \left(\bar{y}_{\cdot j} - \bar{y}_{\cdot\cdot}\right)\sum_{i=1}^{n_j}\left(y_{ij} - \bar{y}_{\cdot j}\right) + \sum_{i=1}^{n_j}\left(\bar{y}_{\cdot j} - \bar{y}_{\cdot\cdot}\right)^2\right)}{n_{tot}} \\
&= \sum_{j=1}^{J} \frac{\sum_{i=1}^{n_j}\left(y_{ij} - \bar{y}_{\cdot j}\right)^2 + 2 \times \left(\bar{y}_{\cdot j} - \bar{y}_{\cdot\cdot}\right) \times 0 + \sum_{i=1}^{n_j}\left(\bar{y}_{\cdot j} - \bar{y}_{\cdot\cdot}\right)^2}{n_{tot}} \\
&= \sum_{j=1}^{J} \frac{\sum_{i=1}^{n_j}\left(y_{ij} - \bar{y}_{\cdot j}\right)^2 + \sum_{i=1}^{n_j}\left(\bar{y}_{\cdot j} - \bar{y}_{\cdot\cdot}\right)^2}{n_{tot}} \\
&= \sum_{j=1}^{J} \frac{\left(n_j - 1\right)s_j^2}{n_{tot}} + \sum_{j=1}^{J} n_j \frac{\left(\bar{y}_{\cdot j} - \bar{y}_{\cdot\cdot}\right)^2}{n_{tot}}
\end{aligned}
\tag{10}
$$

where

$$s_j^2 \equiv \sum_{i=1}^{n_j} \frac{\left(y_{ij} - \bar{y}_{.j}\right)^2}{n_j - 1}$$

is the sample standard deviation of the $j$th peak.

This corresponds to Evans' Eq 25. Our first term, the mean within peak sum of squares, corresponds to his second. Our second term, the mean between peak sum of squares, corresponds to his first. However, we did not assume that the expectation of the $j$ th distribution is the $j$ th bright spot location, we did not conclude that the average of the expectations of the distributions for the $j$ faces is constant ($\pi/2$ for the right half-profile in his coordinate system), and we handled the case of nonreflection.

Evans argues that the first term on the right hand side (RHS) of Eq 10 can be approximated by $\sigma^2/\cos(\mu)$ where $\mu$ is the MFA and $\sigma^2$ is the variability of the MFA. He also argues that the second term on the RHS of Eq 10 can be approximated by $\mu^2/2$. These approximations can be poor and can lead to biased MFA estimates.

Consider the first term on the RHS of Eq 10. To approximate it, Evans made use of his Eq 14, which is $\delta_j = \sigma \sec\left(\mu \sin\left(\alpha_j - \theta\right)\right)$ where $\theta$ is the Bragg angle, $\delta_j$ is the standard deviation of the $j$ th intensity peak in the half-profile, $\mu$ is the mean of the MFA distribution, and $\sigma$ is the standard deviation of the MFA distribution. For the $j$ th face of the cell, $j = 0, 1, \cdots, J-1$, $\alpha_j = \alpha_0 + 2\pi j/J$ where $\alpha_0$ is the rotation of the cell front face away from perpendicular to the incoming X-ray beam. (Thus, $\alpha_0 = 0$ for a front face that is perpendicular to the incoming X-ray beam.) His Eq 14 can yield seriously inflated estimates of $\delta_j$. This can be established heuristically, by simulation, and analytically.

The heuristic argument is based on Figure 5. This figure displays the locations of the eight bright spots on the back plane for a cell with rectangular cross-section in the no rotation, no tilt case. Figure 5 shows that as MFA varies, locations of bright spots associated with wood cell front and back faces vary much more than do locations of bright spots associated with the right and left faces. However, as Evans notes, his Eq 14 predicts that bright spots associated with right and left faces will be broadened more than bright spots associated with front and back faces.

Our simulation estimates of the variabilities of each broadened bright spot are reported in Tables 6-10 and 31-35 of Verrill et al (2010b) and support our heuristic understanding. Estimates of the $\delta_j$'s based on Evans' Eq 14 frequently significantly exceed simulation estimates.

Finally, it is possible to obtain analytic estimates of $\delta_j$'s. This approach is described in Appendix C of Verrill et al (2010a). It is based on a Taylor series approximation and will be most accurate for smaller MFAs. These analytic estimates of $\delta_j$'s were also reported in Tables 6-10 and 31-35 of Verrill et al (2010b), and they agree with our simulation estimates for smaller MFAs. The resulting upward bias in $\sigma^2/\cos(\mu)$ as an estimate of $\sum_{j=1}^{J}\left(n_j - 1\right)s_j^2/n_{tot}$ was reported in Tables 11-15 and 36-40 of Verrill et al (2010b).
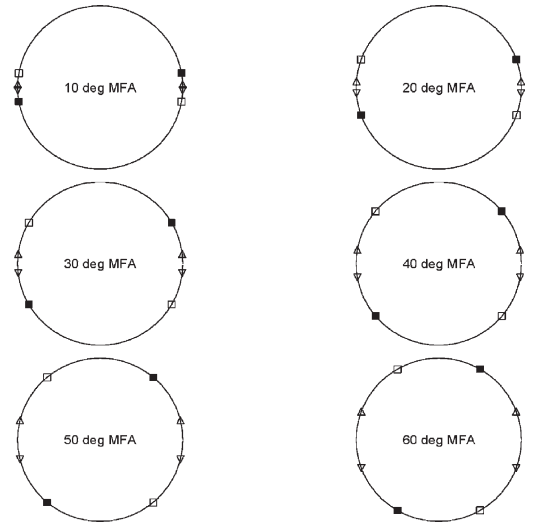


Figure 5.   Locations of high-intensity X-ray spots on the back plane for wood cell tilt = 0° and wood cell rotation = 0°. Open squares represent spots caused by the front (before tilt and rotation) face. Filled squares represent spots caused by the back face. Triangles pointing up represent spots caused by the right face. Triangles pointing down represent spots caused by the left face (MFA, microfibril angle).

This bias can be quite large. For example, for a rectangular cell cross-section, 0° rotation, and 0° tilt, percentage bias ranged from 89-123% as MFA ranged from 2-55°. For a hexagonal cell cross-section, 0° rotation, and 0° tilt, percentage bias ranged from 95-39% as MFA ranged from 2-55°.

Now consider the second term on the RHS of Eq 10. Evans argued that it is approximately equal to $\mu^2/2$. (It might be argued that the term Evans is approximating, $\sum_{j=1}^{J}(\phi_j - \bar{\phi})^2/J$, differs from our $\sum_{j=1}^{J} n_j(\bar{y}_{\cdot j} - \bar{y}_{\cdot\cdot})^2/n_{tot}$. However, in our simulations, we showed that $\mu^2/2$ is also a poor approximation to $\sum_{j=1}^{J}(\phi_j - \bar{\phi})^2/J$.) In fact, $\mu^2/2$ almost always underestimated the second term on the RHS of Eq 10, sometimes severely. Again, it is possible to obtain an intuitive feel for this underestimation. It is well known (Cave 1966; Verrill et al 2006) that for cells with rectangular cross-section in the no rotation, no tilt case, the azimuthal angles (in our coordinate system) of the bright spot locations for front and back faces in the left half-profile (LHP) are $-\mu$ and $\mu$, and the azimuthal angle of the center of the bright spots is 0. (In our 2006 article, we define $\phi = 0$ to correspond to the eastern direction on the back plane (as does Cave 1966). Evans takes the northern direction as $\phi = 0$. In our coordinate system, the center of the left intensity half-profile (corresponding to right side of back plane) will tend to be located near our $\phi = 0$ and the center of the right intensity half-profile (corresponding to left side of the back plane) will tend to be located near our $\phi = \pi$. In Evans' coordinate system, these centers will be at approximately $-\pi/2$ and $+\pi/2$.) Thus, we would expect that $\sum_{j=1}^{J} n_j(\bar{y}_{\cdot j} - \bar{y}_{\cdot\cdot})^2/n_{tot}$ is at least equal to $(-\mu - 0)^2 + (\mu - 0)^2/4 = \mu^2/2$. However, as we can see from Fig 5, the bright spots associated with the right and left faces were symmetric around 0 and not equal to 0. Thus, $\sum_{j=1}^{J} n_j(\bar{y}_{\cdot j} - \bar{y}_{\cdot\cdot})^2/n_{tot}$ was inflated above $\mu^2/2$ by approximately the amount $\phi_{RL}^2/2$ where the bright spots associated with the right and left faces were located at $\pm\phi_{RL}$ (for the LHP). In

Tables 16-20 and 41-45 of Verrill et al (2010b), we supplemented this heuristic argument with simulation results that indicated $\mu^2/2$ can seriously underestimate the second term on the RHS of Eq 10. For example, for a rectangular cross-section, 45° rotation, and 0° tilt, percentage biases ranged from –5 to –35% as MFA ranged from 2-55°. For a hexagonal cross-section, 0° rotation, and 0° tilt, percentage biases ranged from –7 to –30% as MFA ranged from 2-55°.

There are two additional indications that the theory that leads to Eq 1 is not fully satisfactory. First, the theory draws no distinction between LHP and right half-profile (RHP). That is, according to the theory, it should not matter whether the $S^2$ used in Eq 1 is the variance of the LHP, the variance of the RHP, or their average. However, it does matter. For example, for a rectangular cross-section, 0° tilt, and 15° rotation (Table 21 in Verrill et al 2010b), there was a 4.1° difference between LHP and RHP biases for a 40° MFA and a 10.5° difference for a 50° MFA. Second, in the final approximation for $S^2$, cell rotation was not included as a predictor. That is, according to the theory, cell rotation should not matter. However, it does matter. For example, for a rectangular cross-section, 0° tilt, and 40° MFA (Table 21 in Verrill et al 2010b), as rotation increased from 0-45°, MFA bias increased from –0.1 to 4°. For MFA of 50°, as rotation increased from 0-45°, MFA bias increased from 1.7-9.2 degrees.

The net result of the variance approach's overestimation (in general) of the first term on the RHS of Eq 10 and its underestimation (in general) of the second term on the RHS of Eq 10 is that as MFA increases, bias in the variance approach estimate of MFA increases (Tables 21-25 and 46-50 and Figs 2-29 of Verrill et al 2010a). For rectangular cross-sections, in the no cell rotation, no tilt case, bias is always reasonable. (In our simulation, bias increased from –2 to 1.8° as MFA increased from 2 to 55°.) However, in other cases, it is not. For example, for a rectangular cross-section, 15° rotation, 20° tilt, and 40° MFA, full-profile bias (using both sets of peaks—$S^2$ in Eq 1 is replaced by $(S_L^2 + S_R^2)/2$

where $S_L^2$ is LHP variance and $S_R^2$ is RHP variance) was 5.9°, a 15% upward bias. LHP bias (using only the left set of peaks) was 10.1°, a 25% bias. For a hexagonal cross-section, 0° rotation, 20° tilt, and 40° MFA, bias (both full-profile and half-profile) was 7.1°, an 18% bias.

However, the variance approach was not designed to handle tilt. Thus, to be fair to it, in this section, we should focus only on biases in those cases in which tilt was set to 0°. As seen in Table 21 and Figs 2-8 of Verrill et al (2010b), in the 0 tilt case, for rectangular cross-sections and true MFAs between 2 and 55°, full-profile biases increase as MFA increases, do not exceed 11.7° in absolute value, and are largest for a rotation of 45°. Furthermore, it could be argued that the only "significant" biases are associated with MFAs that are 40° or larger.

### EFFECT OF TILT

As noted previously, the variance approach was not designed to handle tilt. Evans (1999) writes: "If the fibre axis is not perpendicular to the X-ray beam, the azimuthal diffraction profile is distorted and MFA is overestimated. Simple methods for the determination of the direction of the fibre axis from the diffraction pattern, and for the correction of the MFA will be presented in a future paper."

Buksnowitz et al (2008) states that "X-ray diffractometry has long been used to estimate grain angle", and it references Evans et al (1996, 1999, 2000). Evans et al (2000) states that "we measure the distortion [in the diffraction pattern] to correct the MFA results for the effects of fibre tilt in the beam direction . . . A description of the method will be presented in a future report." It also states that the "relative orientations of the fibres within the samples were measured using X-ray diffractometry (R. Evans, manuscript in preparation)." Thus, Evans and others claim to have developed extensions to the variance approach that permit tilt to be properly handled. However, no article has yet appeared in the literature that details these methods. In the absence of publicly available

algorithms for correcting the variance approach method for tilt, it is worthwhile to investigate the effect of tilt on bias in estimates. In Tables 21-25 and 46-50 and Figs 2-8 and 16-22 of Verrill et al (2010b), we see that bias in full-profile variance approach estimates increases as tilt increases and that it can be quite large. We present a subset of these biases in Tables 1 and 2. These biases are among the worst that appear in the full set of tables. We expect that other diffractometric methods of estimating MFA are also likely to perform poorly in the presence of larger tilt if they are not corrected for tilt.

### SOURCES OF ROTATION AND TILT

There are two sources of nonnominal tilts and rotations. One stems from faulty specimen preparation. This source can be minimized by proper quality control. The second source is associated with natural variability and is much more difficult to control.

Table 1. Selected full-profile biases in the variance approach estimates for a rectangular cross-section (examples of worst biases).[a]

| Tilt | Rotation | MFA | Bias |
|---|---|---|---|
| 20.0 | 30.0 | 2.0 | −2.0 |
| 20.0 | 30.0 | 10.0 | −0.9 |
| 20.0 | 30.0 | 20.0 | 0.8 |
| 20.0 | 30.0 | 30.0 | 2.8 |
| 20.0 | 30.0 | 40.0 | 6.6 |
| 20.0 | 30.0 | 50.0 | 11.9 |
| 20.0 | 30.0 | 55.0 | 15.1 |
| 30.0 | 15.0 | 2.0 | −2.0 |
| 30.0 | 15.0 | 10.0 | 0.4 |
| 30.0 | 15.0 | 20.0 | 2.5 |
| 30.0 | 15.0 | 30.0 | 6.2 |
| 30.0 | 15.0 | 40.0 | 12.0 |
| 30.0 | 15.0 | 50.0 | 19.2 |
| 30.0 | 15.0 | 55.0 | 23.2 |
| 40.0 | 15.0 | 2.0 | −2.0 |
| 40.0 | 15.0 | 10.0 | 2.6 |
| 40.0 | 15.0 | 20.0 | 6.4 |
| 40.0 | 15.0 | 30.0 | 13.0 |
| 40.0 | 15.0 | 40.0 | 21.4 |
| 40.0 | 15.0 | 50.0 | 28.7 |
| 40.0 | 15.0 | 55.0 | 31.7 |

[a] Lower tilts will yield lower biases. See Tables 21-25 in Verrill et al (2010b) for the complete set of tables.

MFA, microfibril angle.

Table 2. Selected full-profile biases in the variance approach estimates for a hexagonal cross-section (examples of worst biases).[a]

| Tilt | Rotation | MFA | Bias |
| --- | --- | --- | --- |
| 20.0 | 0.0 | 2.0 | −2.0 |
| 20.0 | 0.0 | 10.0 | −0.7 |
| 20.0 | 0.0 | 20.0 | 0.8 |
| 20.0 | 0.0 | 30.0 | 3.2 |
| 20.0 | 0.0 | 40.0 | 7.1 |
| 20.0 | 0.0 | 50.0 | 12.8 |
| 20.0 | 0.0 | 55.0 | 16.1 |
| 30.0 | 0.0 | 2.0 | −2.0 |
| 30.0 | 0.0 | 10.0 | 0.8 |
| 30.0 | 0.0 | 20.0 | 3.2 |
| 30.0 | 0.0 | 30.0 | 7.2 |
| 30.0 | 0.0 | 40.0 | 13.0 |
| 30.0 | 0.0 | 50.0 | 19.6 |
| 30.0 | 0.0 | 55.0 | 22.7 |
| 40.0 | 0.0 | 2.0 | −0.5 |
| 40.0 | 0.0 | 10.0 | 3.0 |
| 40.0 | 0.0 | 20.0 | 7.7 |
| 40.0 | 0.0 | 30.0 | 15.0 |
| 40.0 | 0.0 | 40.0 | 22.6 |
| 40.0 | 0.0 | 50.0 | 29.3 |
| 40.0 | 0.0 | 55.0 | 31.2 |

[a] Lower tilts will yield lower biases. See Tables 46-50 in Verrill et al (2010b) for the complete set of tables.

MFA, microfibril angle.

In Fig 6, we illustrate sample preparation problems that can be controlled. First (Fig 6a), cores that are not perfectly radial (assuming a perfectly cylindrical tree) lead effectively to wood cell rotations. Second (Fig 6b), cores that are not perfectly horizontal lead effectively to $\alpha$ wood cell tilts (Fig 7b defines $\alpha$). Third (Fig 6c), cores that are not correctly finished can lead to $\beta$ wood cell tilts (Fig 7b defines $\beta$). Fourth (Fig 6d-f), finished cores that are not properly aligned in the X-ray apparatus can yield rotations and tilts. (We note that in the absence of accompanying wood cell rotations, $\alpha$ tilts simply rotate the back plane pattern and might not yield significantly biased estimates of MFA. See figs 8 and 15 of Verrill et al 2010a.) For their measurements to be valid, system developers that use an unmodified variance approach need to develop quality control procedures that minimize tilt.

In Fig 7, we illustrate natural variability problems that are more difficult to control. Figure 7a shows that noncylindrical growth can yield cell

rotations even when cores are perfectly radial. Figure 7b illustrates potential, naturally occurring wood cell tilts. Sarén et al (2006) found that in Norway spruce, $\alpha$ tilt in Fig 7b tended to gradually increase from small negative angles (−6 to 0°) near the pith toward small positive angles (0 to 6°) near the bark, and that $\beta$ tilt (spiral grain) can be cyclical with absolute values ranging from 0 to 30°. Buksnowitz et al (2008) found that in Norway spruce, $\beta$ tilt can vary from −11 to +12°. For *Eucalyptus nitens* (H. Deane & Maiden) Maiden trees, Evans et al (2000) reported a "standard deviation of fibre axial orientation" that ranged from approximately 13-16.5°. Given that their fiber axial orientation included both "roll" ($\alpha$) and "pitch" ($\beta$), it is unclear how "standard deviation of fibre axial orientation" was calculated. However, it appears that the $\beta$ range could have been quite large. (They remarked that "Fibre pitch variation was consistently greater than roll variation.") Gindl and Teischinger (2002) studied blocks from 12 larch trees and found spiral grain angles that ranged from 0-40°. Angles between 0 and 5° were most common, but angles greater than 20° were not uncommon (See their Fig 2.). However, the authors noted that "material was selected specifically to represent an optimum variability of grain angle." Northcott (1957) found spiral grain angles that varied from −16 to 19° in Douglas-fir. Houkal (1982) found that the absolute value of spiral grain ranged from 0-16° in *Pinus oocarpa* Schiede ex Schltdl. Martley (1920) studied 19 Indian hardwoods and found spiral grain angles that varied from −33 to +35°. Noskowiak (1963) observed spiral grain angles as large as 40° in mature foxtail pine (*Pinus balfouriana* Grev. and Balf.).

We performed exploratory studies (described in detail in Appendix H of Verrill et al 2010a) that indicated that in samples from *Pinus lambertiana* Dougl. and *Pinus monticola* Dougl. ex D. Don., natural variability in cell rotation has mean roughly equal to 0° and standard deviation roughly equal to 5°. In a sample of 220 cells from *Pinus lambertiana*, the range of rotations was from −17 to +15°. In a sample
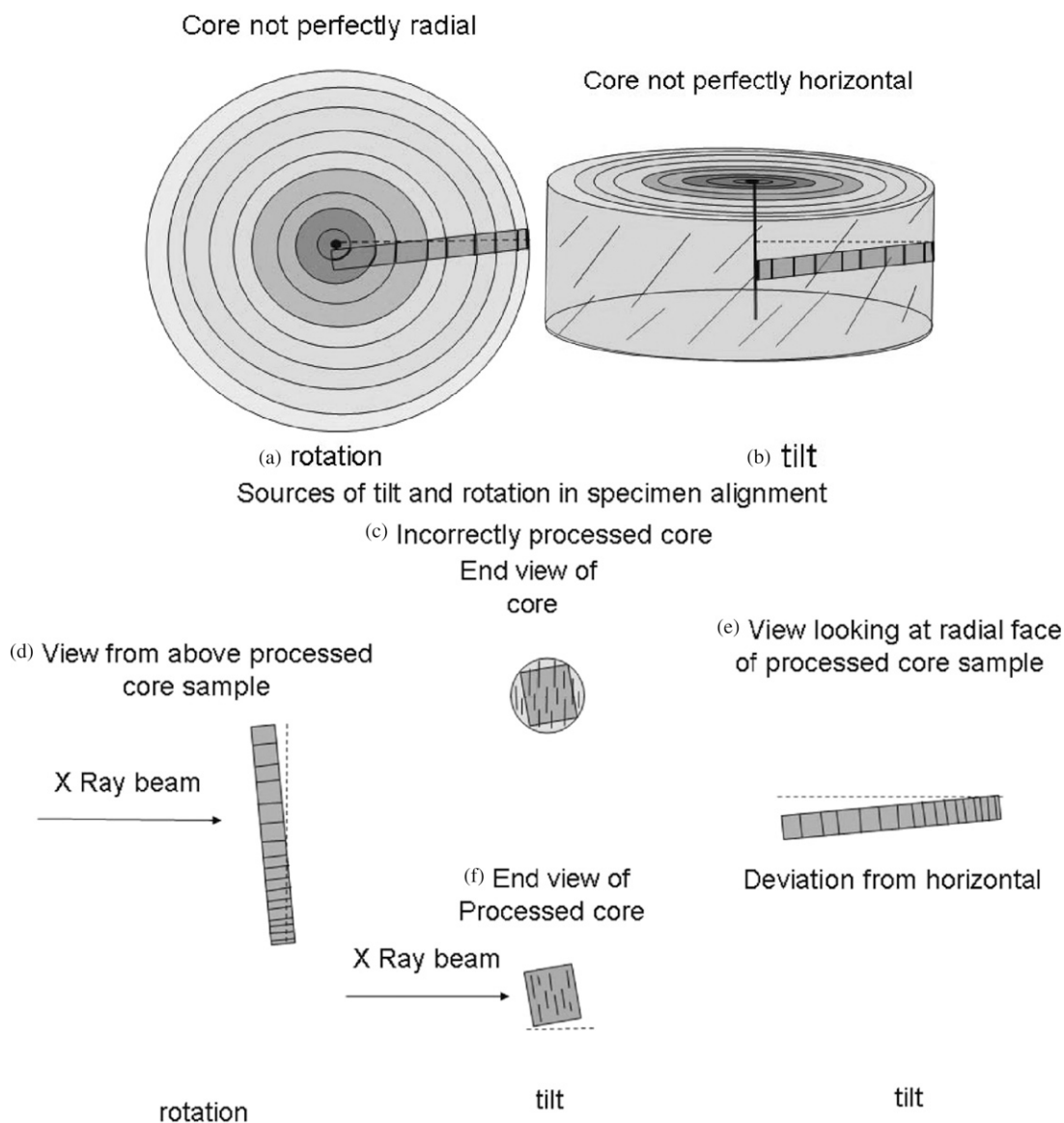
## Core not perfectly radial

Core not perfectly horizontal

(a) rotation (b) tilt

Sources of tilt and rotation in specimen alignment

(c) Incorrectly processed core

End view of core

(e) View looking at radial face of processed core sample

(d) View from above processed core sample

X Ray beam

(f) End view of Processed core

X Ray beam

Deviation from horizontal

rotation tilt tilt

Figure 6. (a) Cell rotation caused by a nonperfectly radial core. (b) Cell $\alpha$ tilt caused by a nonperfectly horizontal core. (c-f) Cell rotation and $\alpha$ and $\beta$ tilts caused by incorrect processing of core and misalignment of processed core.

of 243 cells from *Pinus monticola*, the range of rotations was from –25 to +14°. We observed no trend in mean rotation as we progressed from pith to bark.

In this study, we also found that cells were primarily quadrilateral (40.2%), hexagonal (34.1%), elliptical (16.8%), and pentagonal (8.6%) in cross-section. Earlywood percentages differ from latewood percentages (Appendix H of Verrill et al 2010a). Also note that for hexagonal cells viewed from the tangential face, the default rotation is 0°, whereas for hexagonal cells viewed from the radial face, the default rotation is 30°.
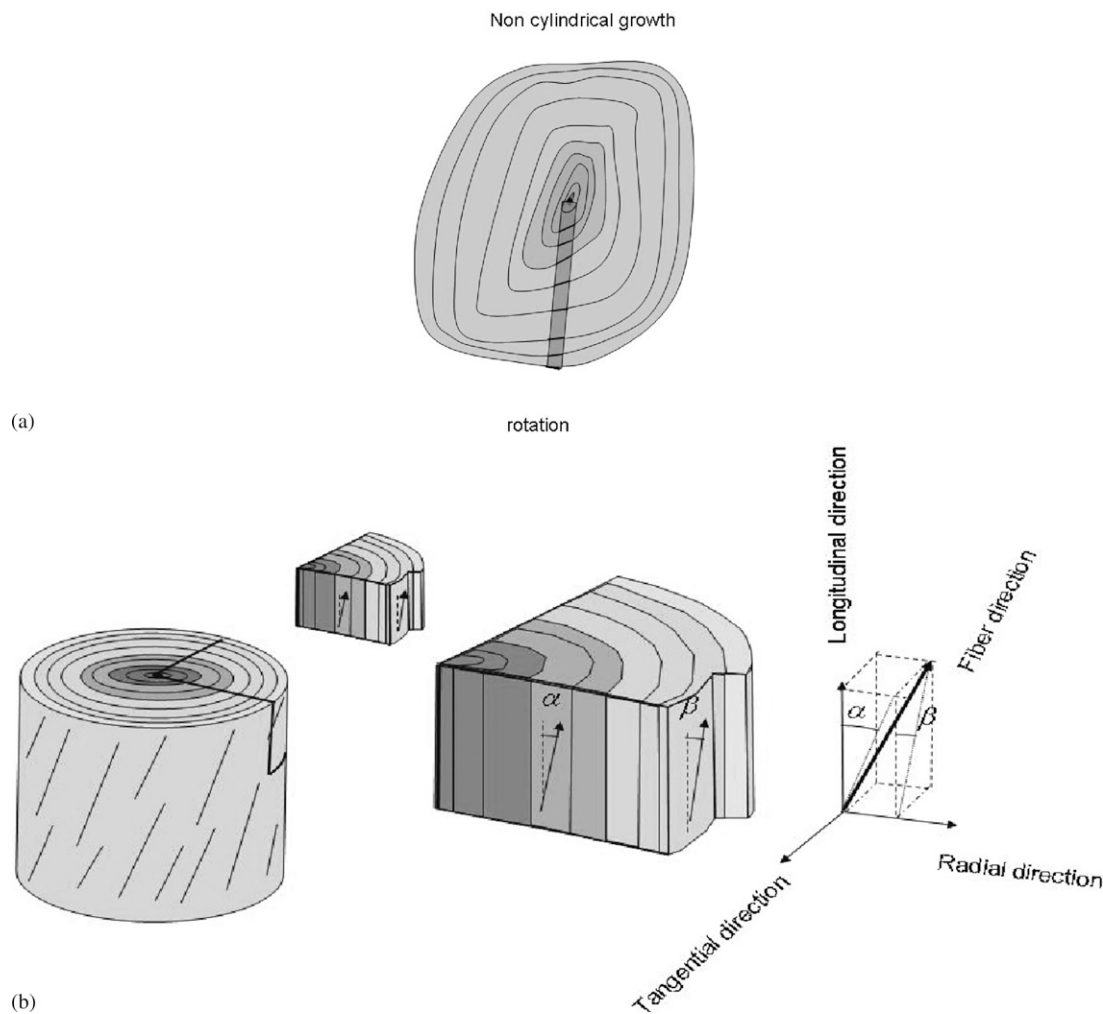
Non cylindrical growth



(a)

rotation



(b)

Figure 7.    (a) Cell rotation caused by noncylindrical growth. (b) Natural $\alpha$ and $\beta$ (spiral growth) tilts.

### ESTIMATING $\sigma^2$ AS A FUNCTION OF MICROFIBRIL ANGLE

As noted previously, the variance approach is based on two approximations. First,

$$S^2 \approx \frac{\mu^2}{2} + \sigma^2 \qquad (11)$$

where $\mu$ denotes MFA and $\sigma^2$ denotes the natural variability of MFA. Second,

$$\sigma^2 \approx f(\mu) \qquad (12)$$

for some function $f$. Combining the two approximations, we obtain

$$S^2 \approx \frac{\mu^2}{2} + f(\mu)$$

and we can, at least in principle, solve for $\mu$.

We established in our simulations that Eq 11 can lead to significantly biased estimates of $\mu$ even if we know exactly the best $f$ in Eq 12. (In our simulations we knew that the generating variance of the MFAs was $\sigma^2 = (\mu/3)^2 + 6^2$.)

In this section, we discuss possible choices for $f(\mu)$ and demonstrate that, as one would expect, additional biases can occur if the $f$ that one

chooses for a variance approach analysis does not match the generating $f(\mu)$.

As noted previously, Evans (1999, 2008) suggested that $\sigma^2$ could be replaced by

$$\sigma^2 \approx f(\mu) = \left(\frac{\mu}{3}\right)^2 + 6^2 \qquad (13)$$

What is the source of Eq 13? Cave (1966) found that he could obtain a good match between X-ray and iodine stain estimates of MFA if he took

$$\sigma^2 = \left(\frac{\mu}{3}\right)^2$$

Evans (1999) noted that MFA variance is nonzero even when MFA is approximately equal to zero. This led him to propose adding a constant to $(\mu/3)^2$. He argued that experience suggests that $6^2$ is a reasonable value for this constant. Thus, Eq 13 is empirical rather than theoretical in nature.

Is there evidence for other forms of $f(\mu)$? Evans (2009) wrote "It should be noted that there are cases in which residual variance decreases with increasing microfibril angle (when compression wood forms, the microfibril angle is high but its variability tends to be lower than in normal wood)".

Cave and Robinson (1998) reported results for seven specimens in which their estimates of MFA ranged from 1-29 while their estimates of $\sigma$ ranged from 10-14° (11° for 1° MFA, 12° for 29° MFA). This suggests that $\sigma$ does not depend on $\mu$.

Donaldson (1998) found that ring number (1, 5, 10, 15) had no effect on MFA range in tracheid samples of size 25 in radiata pine. Because MFA tends to decline as ring number increases and population standard deviation is proportional to sample range (for samples of constant size), this suggests that $\sigma$ does not decrease as $\mu$ decreases.

Alden and Kretschmann (reported in Verrill et al 2011) used iodine crystallization techniques to obtain optical estimates of MFA from 833 prepared slides. Each slide contained cells from earlywood or latewood of a single ring. The first

eight rings from each of two bolts from each of two trees at 26 loblolly pine plantations were evaluated in the study. Alden and Kretschmann measured 10 MFA on each slide. In Fig 8, we plot the standard deviations of the 10 replicates vs the means of the 10 replicates for all 833 slides.

We also plot the $\sigma = \sqrt{(\mu/3)^2 + 6^2}$ line in Fig 8 and the regression line through Alden and Kretschmann's data. There is a clear discrepancy. Of course, variability encountered by X-ray devices can be associated with many hundreds of cells so it would be reasonable for it to be inflated above that measured on the specimen surface. Note, however, the lack of a significant increase in $\sigma$ as a function of $\mu$ in Alden and Kretschmann's data. The slope coefficient in the regression is only 0.04 (with a standard error of 0.009).

Peura et al (2008a) used synchrotron X-ray microdiffraction to investigate the distribution of MFA in single cells. In Fig 9, we plot standard deviations (calculated as 0.425 times their full width at half maximum values) vs mode values for the 17 samples in their Table 3. We also plot the $\sigma = \sqrt{(\mu/3)^2 + 6^2}$ line in Fig 9 and the regression line through the Peura et al (2008a) data. In this case, it appears that Eq 13 underestimates $\sigma$, especially given that the standard deviations plotted in Fig 9 are from single
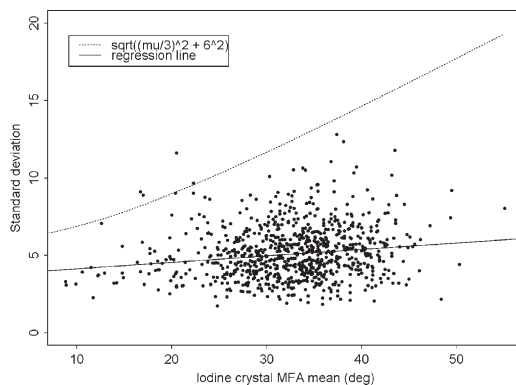


Figure 8.   Microfibril angle (MFA) standard deviation vs iodine crystallization MFA from Alden and Kretschmann (reported in Verrill et al 2011).

cells. On the other hand, there is some support for the idea that $\sigma$ increases as MFA increases. The slope coefficient for the regression line in Fig 9 is 0.19 (with standard error of 0.08).

What kinds of bias can occur if Eq 11 holds but Eq 13 does not? For purposes of illustration, we consider three alternative models. We do not claim that we have strong evidence for any of these models. However, Alden and Kretschmann's results (Verrill et al 2011) are in accord with Model 1, Cave and Robinson (1998) is in accord with Model 2, and Peura et al (2008a) is in accord with Model 3. Our main point is that given the dependence of the bias in the variance approach estimate on the true form for $\sigma^2$, it would be reasonable for implementors of the approach to carefully investigate this relationship. If implementors have already done so and have developed alternative methods for approximating $\sigma^2$ by a function of MFA, we encourage them to publish their new algorithms. This would be useful to other potential implementors.

It is possible that there is no single $f$ that satisfies Eq 12 for all data sets. In this case, to apply the variance approach, one would first have to calibrate each new data source with, for example, an optical method. That is, one would have to use optical methods to determine an $f$ that satisfied Eq 12 for the data source.
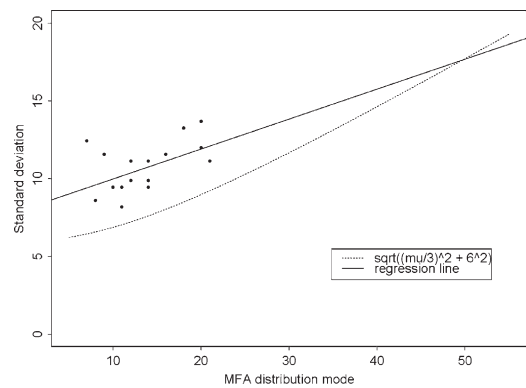


Figure 9. The single cell microfibril angle (MFA) standard deviation (calculated from full width at half maximum values) vs the mode of the single cell MFA distribution. Values from 17 cells (1 obscured). Peura et al (2008a).

Model 1: $\sigma = 5$

In this case, we have

$$\hat{\mu} = \sqrt{\frac{18}{11}} \sqrt{S^2 - 6^2} = \sqrt{\frac{18}{11}} \sqrt{\frac{\mu^2}{2} + 5^2 - 6^2}$$

Biases and percentage biases are reported in Table 3.

Model 2: $\sigma = 12$

In this case, we have

$$\hat{\mu} = \sqrt{\frac{18}{11}} \sqrt{S^2 - 6^2} = \sqrt{\frac{18}{11}} \sqrt{\frac{\mu^2}{2} + 12^2 - 6^2}$$

Biases and percentage biases are reported in Table 4.

Model 3: $\sigma = 8 + \dfrac{\mu}{5}$

In this case, we have

$$\hat{\mu} = \sqrt{\frac{18}{11}} \sqrt{S^2 - 6^2} = \sqrt{\frac{18}{11}} \sqrt{\frac{\mu^2}{2} + \left(8 + \frac{\mu}{5}\right)^2 - 6^2}$$

Biases and percentage biases are reported in Table 5.

### SUMMARY

We have raised concerns about three aspects of the variance approach to estimating MFA.

Table 3. Biases when $S^2 = \mu^2/2 + \sigma^2$, $\sigma^2 = 5^2$, and we incorrectly assume $\sigma^2 = (\mu/3)^2 + 6^2$.

| True MFA ($\mu$) | Estimated MFA ($\hat{\mu}$) | Bias ($\hat{\mu} - \mu$) | Bias (%) |
|---|---|---|---|
| 5 | 1.57 | −3.43 | −68.7 |
| 10 | 7.99 | −2.01 | −20.1 |
| 15 | 12.89 | −2.11 | −14.1 |
| 20 | 17.59 | −2.41 | −12.1 |
| 25 | 22.21 | −2.79 | −11.2 |
| 30 | 26.80 | −3.20 | −10.7 |
| 35 | 31.37 | −3.63 | −10.4 |
| 40 | 35.93 | −4.07 | −10.2 |
| 45 | 40.48 | −4.52 | −10.0 |
| 50 | 45.03 | −4.97 | −9.9 |
| 55 | 49.57 | −5.43 | −9.9 |
| 60 | 54.11 | −5.89 | −9.8 |

MFA, microfibril angle.

First, the approach is based on approximations $S_1^2 \approx \mu^2/2$ and $S_2^2 \approx \sigma^2/\cos(\mu)$ where $S_1^2$ is the mean between peak sum of squares and $S_2^2$ is the mean within peak sum of squares. As we saw previously, biases in these approximations can be quite large, but to some extent, they cancel. Thus, for $0°$ tilts, the maximum full-profile bias that we found for MFAs between 2 and $55°$ was $11.7°$.

Second, we noted that the variance approach was not designed to handle tilt, and consequently, in the presence of tilt, the method can yield highly biased estimates. We also noted that there may be algorithmic fixes for this, but they have not yet appeared in the literature.

Third, as we have seen, there is some doubt about a proper model, $f(\mu)$, for $\sigma^2$. One model proposed by Evans (1999) was $\sigma^2 \approx (\mu/3)^2 + 6^2$. We considered three other models that have some data support and found that there can be large (percent) biases if one of these models is true but $\sigma^2 \approx (\mu/3)^2 + 6^2$ is assumed. This suggests that to apply the variance approach in new situations, it might be necessary to first use optical methods to determine an appropriate $f$ in approximation $\sigma^2 \approx f(\mu)$.

On the other hand, it is important to keep these concerns in perspective. In our simulations, we found that if Eq 4 holds and is used, tilts are restricted to $10°$ or less, and MFAs are restricted to $40°$ or less, then full-profile biases in MFA estimates increase with MFA and do not exceed $4.6°$ in absolute value.

We raise the three concerns so that other researchers interested in understanding, implementing, or extending the variance approach or in comparing the approach to other methods of estimating MFA will be aware of them.

Table 4. Biases when $S^2 = \mu^2/2 + \sigma^2$, $\sigma^2 = 12^2$, and we incorrectly assume $\sigma^2 = (\mu/3)^2 + 6^2$.

| True MFA ($\mu$) | Estimated MFA ($\hat{\mu}$) | Bias ($\hat{\mu} - \mu$) | Bias (%) |
|---|---|---|---|
| 5 | 14.04 | 9.04 | 180.8 |
| 10 | 16.08 | 6.08 | 60.8 |
| 15 | 19.00 | 4.00 | 26.6 |
| 20 | 22.45 | 2.45 | 12.3 |
| 25 | 26.23 | 1.23 | 4.9 |
| 30 | 30.22 | 0.22 | 0.7 |
| 35 | 34.34 | −0.66 | −1.9 |
| 40 | 38.55 | −1.45 | −3.6 |
| 45 | 42.82 | −2.18 | −4.8 |
| 50 | 47.14 | −2.86 | −5.7 |
| 55 | 51.49 | −3.51 | −6.4 |
| 60 | 55.88 | −4.12 | −6.9 |

MFA, microfibril angle.

Table 5. Biases when $S^2 = \mu^2/2 + \sigma^2$, $\sigma = 8 + \mu/5$, and we incorrectly assume $\sigma^2 = (\mu/3)^2 + 6^2$.

| True MFA ($\mu$) | Estimated MFA ($\hat{\mu}$) | Bias ($\hat{\mu} - \mu$) | Bias (%) |
|---|---|---|---|
| 5 | 9.70 | 4.70 | 94.0 |
| 10 | 13.66 | 3.66 | 36.6 |
| 15 | 17.98 | 2.98 | 19.9 |
| 20 | 22.45 | 2.45 | 12.2 |
| 25 | 27.00 | 2.00 | 8.0 |
| 30 | 31.59 | 1.59 | 5.3 |
| 35 | 36.22 | 1.22 | 3.5 |
| 40 | 40.85 | 0.85 | 2.1 |
| 45 | 45.51 | 0.51 | 1.1 |
| 50 | 50.17 | 0.17 | 0.3 |
| 55 | 54.83 | −0.17 | −0.3 |
| 60 | 59.51 | −0.49 | −0.8 |

MFA, microfibril angle.

**REFERENCES**

Buksnowitz C, Müller U, Evans R, Teischinger A, Grabner M (2008) The potential of SilviScan's X-ray diffractometry method for the rapid assessment of spiral grain in softwood, evaluated by goniometric measurements. Wood Sci Technol 42:95-102.

Cave ID (1966) X-ray measurement of microfibril angle. Forest Prod J 16(10):37-42.

Cave ID, Robinson W (1998) Interpretation of (002) diffraction arcs by means of a minimalist model. Pages 108-115 *in* BG Butterfield, ed. Microfibril angle in wood. International Association of Wood Anatomists, University of Canterbury, New Zealand.

Cave ID, Walker JCF (1994) Stiffness of wood in fast-grown plantation softwoods: The influence of microfibril angle. Forest Prod J 44(5):43-48.

Donaldson LA (1998) Between-tracheid variability of microfibril angles in radiata pine. Pages 206-224 *in* BG Butterfield, ed. Microfibril angle in wood. International Association of Wood Anatomists, University of Canterbury, New Zealand.

Evans R (2008) Personal communication.

Evans R (2009) Personal communication.

Evans R, Hughes M, Menz D (1999) Microfibril angle variation by scanning X-ray diffractometry. Appita J 52(5):363-367.

Evans R, Stringer S, Kibblewhite RP (2000) Variation of microfibril angle, density and fibre orientation in twenty-nine Eucalyptus nitens trees. Appita J 53(5):450-457.

Evans R, Stuart SA, Van der Touw J (1996) Microfibril angle scanning of increment cores by X-ray diffractometry. Appita J 49(6):411-414.

Evans RE (1999) A variance approach to the X-ray diffractometric estimation of microfibril angle in wood. Appita J 52(4):283-289, 294.

Evans RE, Illic J (2001) Rapid prediction of wood stiffness from microfibril angle and density. Forest Prod J 51:53-57.

Gindl W, Teischinger A (2002) The potential of Vis- and NIR-spectroscopy for the nondestructive evaluation of grain-angle in wood. Wood Fiber Sci 34(4):651-656.

Harris JM, Meylan BA (1965) The influence of microfibril angle on longitudinal and tangential shrinkage in *Pinus radiata*. Holzforschung 19(5):144-153.

Houkal D (1982) Spiral grain in *Pinus ocarpa*. Wood Fiber Sci 14(4):320-330.

Martley JF (1920) Double cross grain. Ann Appl Biol 7(2-3):224-268.

Megraw RA (1986) Wood quality factors in loblolly pine: The influence of tree age, position in the tree, and cultural practice on wood specific gravity, fiber length and fibril angle. TAPPI Press, Norcross, GA. 88 pp.

Northcott PL (1957) Is spiral grain the normal growth pattern? For Chron 33(4):335-352.

Noskowiak AF (1963) Spiral grain in trees. A review. Forest Prod J 13(7):266-275.

Peura M, Müller M, Serimaa RM, Vainio U, Sarén M, Saranpää P, Burghammer M (2005) Structural studies of single wood cell walls by synchrotron X-ray microdiffraction and polarised light microscopy. Nucl Instrum Meth B. 238:16-20.

Peura M, Müller M, Vainio U, Sarén M, Saranpää P, Serimaa R (2008a) X-ray microdiffraction reveals the orientation of cellulose microfibrils and the size of cellulose crystallites in single Norway spruce tracheids. Trees (Berl) 22:49-61.

Peura M, Sarén M, Laukkanen J, Nygard K, Andersson S, Saranpää P, Paakkari T, Hämäläinen K, Serimaa R (2008b) The elemental composition, the microfibril angle distribution and the shape of the cell cross-section in Norway spruce xylem. Trees (Berl) 22:499-510.

Sarén M, Serimaa R, Andersson S, Paakkari T, Saranpää P, Pesonen E (2001) Structural variation of tracheids in Norway spruce (*Picea abies* [L.] Karst.). J Struct Biol 136:101-109.

Sarén M, Serimaa R (2006) Determination of microfibril angle distribution by X-ray diffraction. Wood Sci Technol 40:445-460.

Sarén M, Serimaa R, Tolonen Y (2006) Determination of fiber orientation in Norway spruce using X-ray diffraction and laser scattering. Holz Roh Werkst 64:183-188.

Verrill SP, Kahaner D, Marsaglia G (2010) Source code for the FORTRAN programs that simulate variance approach estimation of microfibril angle. http://www1.fpl.fs.fed.us/varapp_sim.html (18 March 2011).

Verrill SP, Kretschmann DE, Herian VL (2001) JMFA—A graphically interactive Java program that fits microfibril angle X-ray diffraction data. Res Note FPL-RN-283 USDA For Serv Forest Prod Lab, Madison, WI. 44 pp.

Verrill SP, Kretschmann DE, Herian VL (2006) JMFA 2—A graphically interactive Java program that fits microfibril angle X-ray diffraction data. Res Pap FPL-RP-635 USDA For Serv For Prod Lab, Madison, WI. 70 pp.

Verrill SP, Kretschmann DE, Herian VL, Alden HA (2011) JMFA 3—A graphically interactive Java program that fits microfibril angle X-ray diffraction data. Manuscript in preparation.

Verrill SP, Kretschmann DE, Herian VL, Wiemann MC, Alden HA (2010a) Concerns about a variance approach to the X-ray diffractometric estimation of microfibril angle in wood. Res Pap FPL-RP-658. USDA For Serv For Prod Lab, Madison, WI.

Verrill SP, Kretschmann DE, Herian VL, Wiemann MC, Alden HA (2010b) Tables from the simulation of a variance approach to microfibril angle estimation. http://www1.fpl.fs.fed.us/varapp_tables.html (18 March 2011).